Monoclinic phases arising across thermal inter-ferroelectric phase transitions

Yijia Gu, Fei Xue, Shiming Lei, Tom T. A. Lummen, Jianjun Wang, Venkatraman Gopalan, and Long-Qing Chen
Department of Materials Science and Engineering, The Pennsylvania State University, University Park, Pennsylvania 16802, USA
(Received 26 May 2014; published 31 July 2014)

Thermotropic phase boundaries (TPBs), as thermal analogs of morphotropic phase boundaries (MPBs), are associated with the thermal inter-ferroelectric phase transitions. Similar to an MPB, a TPB exhibits a characteristically flattened energy profile which favors polarization rotation, thus giving rise to a structurally bridging low-symmetry phase. We report on the kinetic process of thermal inter-ferroelectric phase transitions in $BaTiO_3$ and $KNbO_3$ using the phase-field method. The domain structures are found to play key roles in stabilizing the monoclinic phase. In simple domain structures, the monoclinic phase is a transient phase and cannot be stabilized into its neighboring phase regimes. However, by introducing structural inhomogeneity (orthogonal in-plane domain twins), we found that the monoclinic phase can be stabilized over a range of over 100 K across the transition. As a result, the piezoelectric properties are enhanced due to the stabilized monoclinic phase. In addition to the emergence of new piezoelectric components with monoclinic symmetry, most of the original components present in the tetragonal symmetry also show substantial enhancement with the rotation of polarization.

DOI: 10.1103/PhysRevB.90.024104 PACS number(s): 77.80.Dj, 77.80.B−, 77.65.−j

I. INTRODUCTION

Ferroelectrics are materials that exhibit an electric-field-controlled reversible spontaneous electric polarization [1]. Due to the strong electrostrictive coupling between deformation and ferroelectric polarization, most ferroelectrics also exhibit a strong piezoelectric effect, which describes the linear dependence of the deformation on the applied electric field. This property makes ferroelectrics good candidates for microelectromechanical systems [2,3].

The search for ferroelectrics with a strong piezoelectric effect has been an ongoing endeavor, with extensive contributions from both theory and experiments. The commercially widespread and currently best-performing class of piezoelectrics comprises the complex lead-based solid solution materials that exhibit a so-called morphotropic phase boundary (MPB). The MPB is a compositional region connecting two stable ferroelectric phases, and it gives rise to an intermediate phase with strongly enhanced functional properties, such as ultrahigh piezoelectric response [4–7]. The polarization rotation mechanism has been shown to be responsible for the enhancement of the piezoelectric property in MPBs by density-functional theory calculations [5]. However, almost all the current ferroelectric systems with MPBs are lead-based solid solutions. In search for environmentally sustainable alternatives, systems that mimic the principal characteristics [6–9] of MPBs have been pursued by means of solid solution [10], pressure [11], epitaxial strain [12,13], multilayering [14,15], and microstructure engineering [16–18]. From the energetic perspective, all these experimental approaches are essentially flattening the free energy landscape of the different ferroelectric states [19–21], which not only favors polarization rotation, but also greatly increases the dielectric susceptibility. Since the largest achievable piezoelectric coefficients do not necessarily correspond to ferroelectric polarizations oriented along high-symmetry directions in single crystals, stabilizing intermediate low-symmetry phases by flattening the free energy profile between high-symmetry minima may give rise to stronger electromechanical responses, such as in the lead-free perovskites $BaTiO_3$ [22] and $KNbO_3$ [23].

The typical perovskite ferroelectrics exhibit three first-order ferroelectric phase transitions upon heating, sequentially adopting rhombohedral (R), orthorhombic (O), tetragonal (T), and cubic (C) phases, as illustrated in Fig. 1. The phase boundaries associated with the thermal ferroelectric phase transitions have been termed thermotropic phase boundaries (TPBs), after their analogy to both morphotropic phase boundaries and thermotropic liquid crystals [25]. The TPBs between the T and the O phases, and between the O and the R phases exhibit the same characteristics as the MPBs, i.e., a flattened energy profile. The divergence of dielectric properties at the transition temperature is one of the prominent outcomes. In fact, several x-ray diffraction experiments [26–28] have shown that monoclinic phases occur as intermediate or secondary phases in $BaTiO_3$. Moreover, the M_C phase has been stabilized in the thermal regime of the O phase by electric field cooling [27]. Most recently, by cycling bulk single crystals of $BaTiO_3$ and $KNbO_3$ through inter-ferroelectric transitions, Lummen *et al.* [25] found that monoclinic phases can also be stabilized by inherent interactions in multidomain structures, without the use of an external driving force. In this case, the inter-ferroelectric transition exhibits thermotropic behavior; instead of a single, well-defined transition temperature separating the two ferroelectric phases, the phase boundary is expanded to an appreciable temperature range in which the material assumes a (partially) monoclinic phase. This is in direct contrast to the inter-ferroelectric phase transition behavior of a simple system that is formed by a single domain or a multidomain system where the domain walls follow the symmetry-prescribed crystallographic planes. In such simple domain systems, the monoclinic phase corresponds to a transient state that disappears in both the T and the O phase regimes. For convenience of discussion, a multidomain system with orthogonal twins that leads to a significant deviation of the domain wall planes from their symmetry-prescribed crystallographic directions is defined as a *complex domain system*, while the other systems, including single domain or multidomain systems with symmetry-prescribed domain walls, are defined as *simple domain systems*.

In this paper, we employ the phase-field approach to systematically study the monoclinic phase in the classic lead-free perovskite ferroelectrics $BaTiO_3$ and $KNbO_3$ (see Appendix) across thermal ferroelectric phase transitions. In the following, we briefly describe the phase-field model and

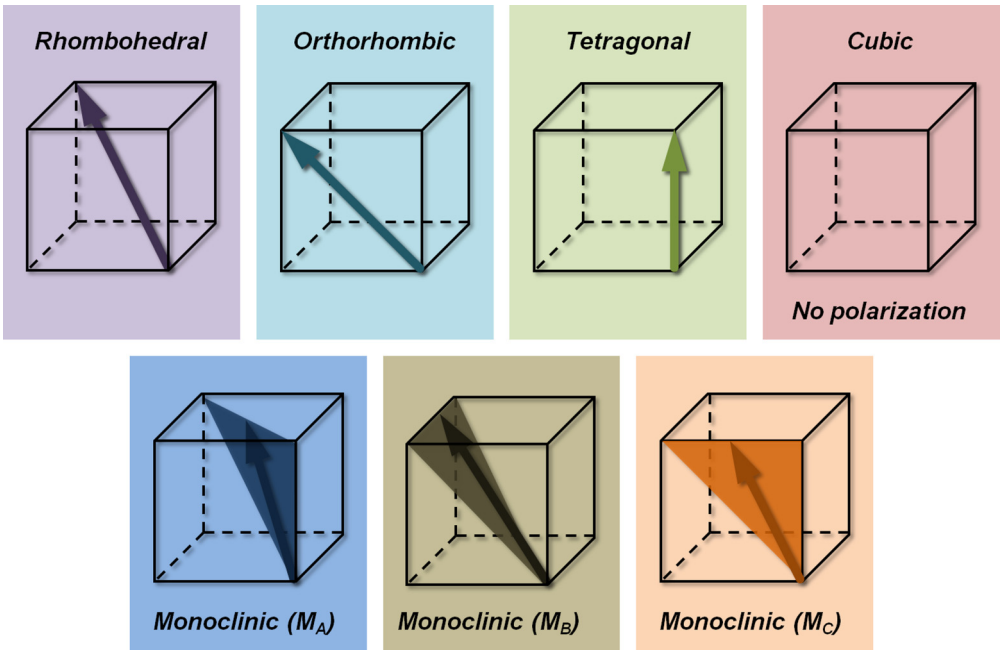

FIG. 1. (Color online) The phase transformation pathway of ROTC perovskite ferroelectrics (from low to high temperature), and three intermediate monoclinic phases M_A, M_B, and M_C. (The classification of monoclinic phases is taken from Ref. [24].) The arrows denote the polarization direction in the Cartesian coordinate system. The shaded triangle in monoclinic phases indicates the ranges in which the polarization direction can vary.

the numerical scheme used for this work in Sec. II, followed by a phase-field simulation of the orthorhombic-tetragonal (O-T) phase transition in a simple domain system, with an emphasis on the kinetic role of M_C phase (M_C disappears in either the T or the O phase regime) in Sec. III. Then, in Sec. IV, we present a comparison study on the complex domain system. We show that rather than a transient intermediate state in the simple domain system, the monoclinic phase can actually be stabilized thermodynamically in the complex domain system, exhibiting extraordinary behavior due to the existence of TPBs. In Sec. V, we present a thorough analysis and discussion of the simulation results from Sec. IV, with an emphasis on the enhanced piezoelectric properties introduced by orthogonal twins in a complex system. Finally, we summarize our study in Sec. VI.

II. PHASE-FIELD MODEL

The phase-field approach is a powerful computational method for studying mesoscale morphological evolution in solid state materials [29]. Based on the Landau-Ginzburg-Devonshire theory, the phase-field approach has been successfully applied to ferroelectric materials in almost every aspect of interest [30]. Details and examples of the phase-field approach can be found in the review papers [29,30], and the references therein.

In our three-dimensional phase-field model, the evolution of the spatial ferroelectric polarization distribution as a function of time is based on the time-dependent Ginzburg-Landau (TDGL) equation

$$\frac{\partial P_i}{\partial t} = -L\left(\frac{\delta F}{\delta P_i}\right) \quad (i = 1,2,3), \tag{1}$$

where P_i is the component of ferroelectric polarization along coordinate i, t is time, L is the kinetic coefficient related to domain wall mobility, and F is the total free energy. In this paper, the pseudocubic coordinate system is assumed. According to the Landau-Ginzburg-Devonshire theory, the total free energy F of ferroelectrics can be written as a functional of polarization P, strain ε, and electric field E, i.e.,

$$F = \int_V [f_{\text{bulk}}(P_i) + f_{\text{elast}}(P_i, \varepsilon_{ij}) + f_{\text{grad}}(\nabla_j P_i) + f_{\text{elec}}(P_i, E_i)]dV \quad (i,j = 1,2,3), \tag{2}$$

where f_{bulk}, f_{elast}, f_{grad}, and f_{elec} are the densities of bulk energy, elastic energy, gradient energy, and electrostatic energy, corresponding to

$$\begin{aligned} f_{\text{bulk}}(P_i) = {} & \alpha_1(T)\left(P_1^2 + P_2^2 + P_3^2\right) + \alpha_{11}\left(P_1^4 + P_2^4 + P_3^4\right) + \alpha_{12}\left(P_1^2P_2^2 + P_2^2P_3^2 + P_3^2P_1^2\right) \\ & + \alpha_{111}\left(P_1^6 + P_2^6 + P_3^6\right) + \alpha_{112}\left[P_1^2\left(P_2^4 + P_3^4\right) + P_2^2\left(P_3^4 + P_1^4\right) + P_3^2\left(P_1^4 + P_2^4\right)\right] \\ & + \alpha_{123}P_1^2P_2^2P_3^2 + \alpha_{1111}\left(P_1^8 + P_2^8 + P_3^8\right) + \alpha_{1122}\left(P_1^4P_2^4 + P_2^4P_3^4 + P_3^4P_1^4\right) \\ & + \alpha_{1112}\left[P_1^6\left(P_2^2 + P_3^2\right) + P_2^6\left(P_3^2 + P_1^2\right) + P_3^6\left(P_1^2 + P_2^2\right)\right] \\ & + \alpha_{1123}\left(P_1^4P_2^2P_3^2 + P_2^4P_3^2P_1^2 + P_3^4P_1^2P_2^2\right), \end{aligned} \tag{3a}$$

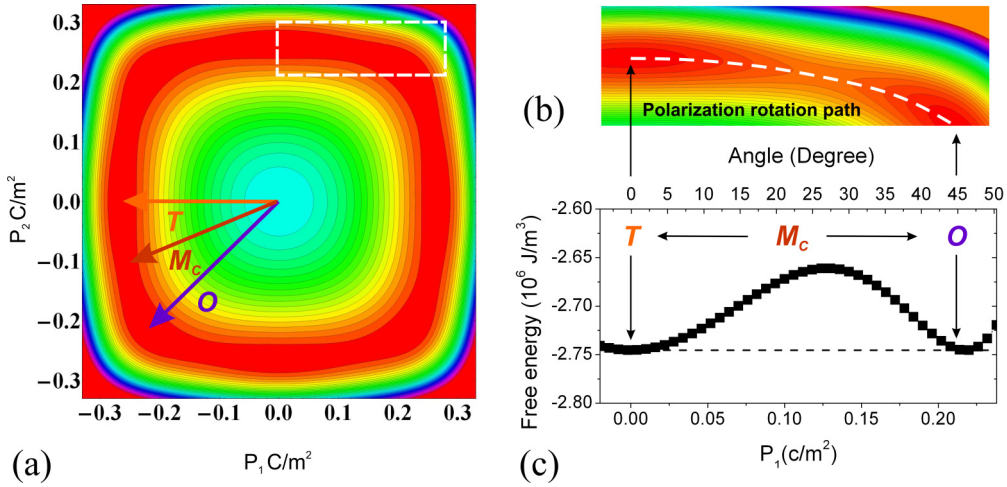

FIG. 2. (Color online) (a) The contour plot of the energy profile of $BaTiO_3$ at the transition temperature (281 K) between T and O. (b) Zoomed-in plot of the T-M_C-O region as indicated by the white dashed box in (a). The white dashes represent the polarization rotation path from T to O. (c) The lowest free energy as a function of P_1 from T to O as indicated by the white dashes in (b).

$$f_{\text{elast}}(P_i,\varepsilon_{ij}) = \frac{1}{2}c_{11}\left(\varepsilon_1^2+\varepsilon_2^2+\varepsilon_3^2\right) + c_{12}(\varepsilon_1\varepsilon_2+\varepsilon_2\varepsilon_3+\varepsilon_3\varepsilon_1) + \frac{1}{2}c_{44}(\varepsilon_4^2+\varepsilon_5^2+\varepsilon_6^2)$$
$$- q_{11}\left(\varepsilon_1 P_1^2+\varepsilon_2 P_2^2+\varepsilon_3 P_3^2\right) - 2q_{44}(\varepsilon_4 P_2 P_3+\varepsilon_5 P_3 P_1+\varepsilon_6 P_1 P_2)$$
$$- q_{12}\left[\varepsilon_1\left(P_2^2+P_3^2\right)+\varepsilon_2\left(P_3^2+P_1^2\right)+\varepsilon_3\left(P_1^2+P_2^2\right)\right], \tag{3b}$$

$$f_{\text{elec}}(P_i,E_i) = -\left(E_1^{\text{ext}}P_1+E_2^{\text{ext}}P_2+E_3^{\text{ext}}P_3\right) - \frac{1}{2}\left(E_1^d P_1+E_2^d P_2+E_3^d P_3\right), \tag{3c}$$

$$f_{\text{grad}}(\nabla_j P_i) = \frac{1}{2}g_{11}\left[\left(\frac{\partial P_1}{\partial x_1}\right)^2+\left(\frac{\partial P_2}{\partial x_2}\right)^2+\left(\frac{\partial P_3}{\partial x_3}\right)^2\right] + g_{12}\left(\frac{\partial P_1}{\partial x_1}\frac{\partial P_2}{\partial x_2}+\frac{\partial P_2}{\partial x_2}\frac{\partial P_3}{\partial x_3}+\frac{\partial P_3}{\partial x_3}\frac{\partial P_1}{\partial x_1}\right)$$
$$+\frac{1}{2}g_{44}\left[\left(\frac{\partial P_1}{\partial x_2}+\frac{\partial P_2}{\partial x_1}\right)^2+\left(\frac{\partial P_2}{\partial x_3}+\frac{\partial P_3}{\partial x_2}\right)^2+\left(\frac{\partial P_3}{\partial x_1}+\frac{\partial P_1}{\partial x_3}\right)^2\right], \tag{3d}$$

where the α are the Landau-Devonshire coefficients, the c_{ij} are the elastic stiffness constants, the q_{ij} are the electrostrictive constants, the g_{ij} are the gradient energy coefficients, E^{ext} is the external electric field, and E^d is the depolarization field. Among all the coefficients, only $\alpha_1(T)$ depends on temperature, obeying the Curie-Weiss law. The phase-field parameters for $BaTiO_3$ and $KNbO_3$ were taken from Refs. [31] and [32], respectively.

To simulate the naturally occurring TPB effect in freestanding ferroelectric crystals, the stress-free boundary condition is assumed, i.e., $\sigma_{ij} = 0$. The stress and strain are calculated by applying microelasticity theory [33]. The depolarization electric field E^d is obtained by solving the electrostatic equilibrium equation $\nabla_i D_i = 0$, where $D_i = \varepsilon_0\kappa_{ij}E_j + P_j$ is the electric displacement with ε_0 the dielectric permittivity of a vacuum and κ_{ij} the background dielectric permittivity [34–36]. The TDGL equations (1) are solved using the semi-implicit Fourier spectral method [37] on a discretized mesh with periodic boundary conditions imposed along all the three directions.

III. TRANSIENT MONOCLINIC PHASE IN SIMPLE DOMAIN SYSTEMS

In this section, we choose the T-O phase transition in $BaTiO_3$ single crystals as an example to study the existence of intermediate monoclinic phases. Figure 2(a) shows the contour plot of the free energy profile of $BaTiO_3$ as a function of two mutual perpendicular polarization components P_1 and P_2 at the transition temperature (281 K) between T and O. The energy well is quite flat as denoted in the zoomed-in plot in Fig. 2(b). The O and T phases are energetically identical, and the monoclinic (M_C) phase has a slightly higher energy ($<1\times10^5$ J/m^3), which can be easily overcome by external strain (~0.1%) or an electric field (~4×10^5 V). Therefore, the bridging monoclinic phases M_A (between R and T), M_B (between O and R), and M_C (between T and O), as illustrated in Fig. 1, are plausible to appear as intermediate states across thermal ferroelectric phase transitions.

To study the microstructural evolution during the thermal T-O ferroelectric phase transition, we apply the phase-field model to $BaTiO_3$ single crystals. For simplicity, we

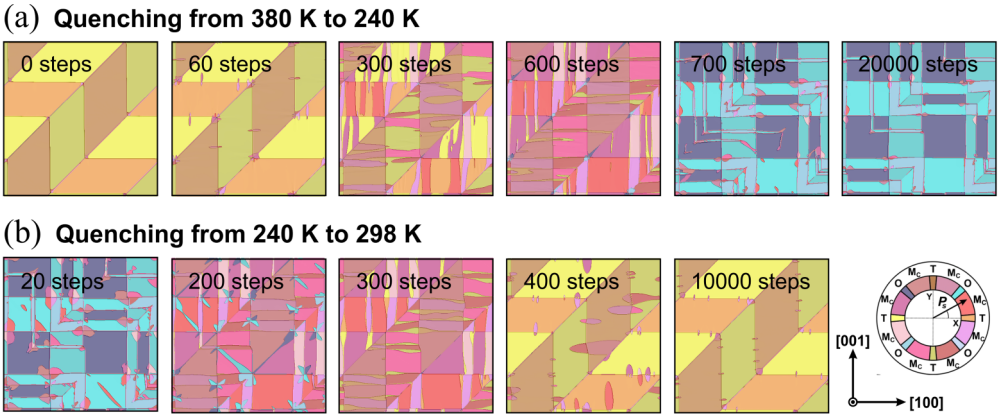

FIG. 3. (Color online) The simple domain structure evolution between the T phase and O phase during temperature cycling. (a) Quenching from 380 K (T regime) to 240 K (O regime); (b) quenching from 240 K (O regime) to 298 K (T regime).

consider only in-plane domain structures, and thus a quasi-two-dimensional (quasi-2D) simulation system is adequate to illustrate the ferroelectric polarization rotation during this process. The discretized quasi-2D simulation size is $512\Delta x \times 512\Delta x \times 4\Delta x$, with a grid spacing of $\Delta x = 1.8$ nm. Due to the quasi-2D nature of the simulations, all domain structures and resulting properties are homogeneous along the out-of-plane direction. We initially started in the thermal T regime with a multidomain configuration at 380 K, which exhibits both 180° domain walls and 90° domain walls at equilibrium. By quenching the temperature of the system to 240 K, in the O regime, we first investigate the microstructural evolution during this process.

Figure 3(a) shows the structural evolution during the T-to-O transition. The thermal ferroelectric phase transition follows exactly the same sequential mechanism as the domain switching induced by an external electric field described in [38]: (i) nucleation at the interface, (ii) forward growth of a needle-like domain, and (iii) sidewise expansion and coalescence of the domains. Initially (0 steps), only T domains with both 90° and 180° domain walls are present in the system. Then, 60 steps after quenching the temperature of the system, several small new phases nucleate at the domain walls. As denoted by the discrete color scale, the spontaneous polarizations (P_s) of these nucleated phases significantly deviate (>5°) from the equilibrium T and O directions, indicating they correspond to M_C phases. Based on the direction of the in-plane polarization P_s, the M_C phase can be categorized into eight different domain variants as illustrated by the color wheel in Fig. 3. To minimize the electrostatic energy, each M_C variant has its preferred growth direction, which is perpendicular to the P_s direction of the original T phase. After 300 steps, the resulting M_C stripes have grown through the original T domains and reached the opposing domain wall. The obtained domain structures are very similar to those previously simulated for an MPB system, although in that case the monoclinic phase was stabilized at low temperatures [39]. In this case, after reaching the opposing domain wall the growth of M_C phase becomes sideways. After 600 steps, almost the entire system has transformed to the intermediate M_C configuration. Then, rapidly following this (at ~700 steps), the system suddenly transforms to the O phase, leaving only a few percent of M_C phase at the domain walls. After 20 000 steps, the system reaches near equilibrium, consisting almost entirely of O domains, with only small M_C domains located at the domain wall junctions. The volume fractions of different phases as a function of time steps are plotted in Fig. 4(a). In this domain configuration, the M_C phase is clearly a transitional phase, which exists only as a

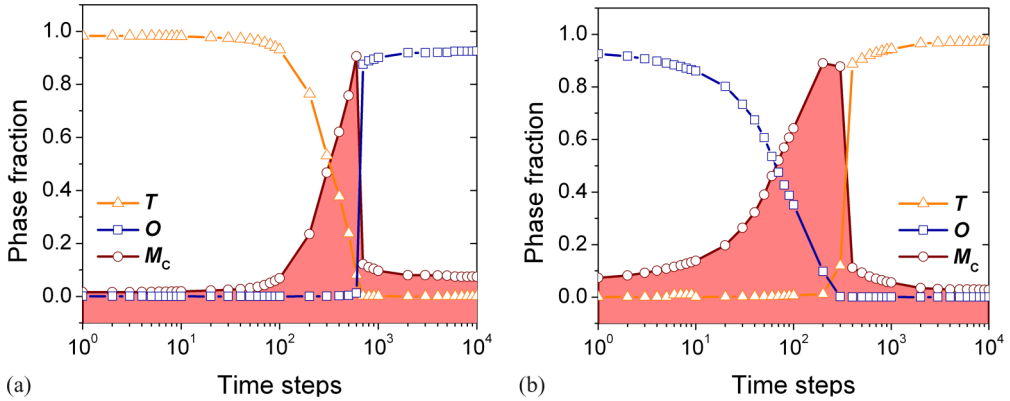

FIG. 4. (Color online) Volume fraction evolution of simple domain system in $BaTiO_3$ during the temperature cycling. (a) Cooling from 380 to 240 K. (b) Heating from 240 to 298 K.

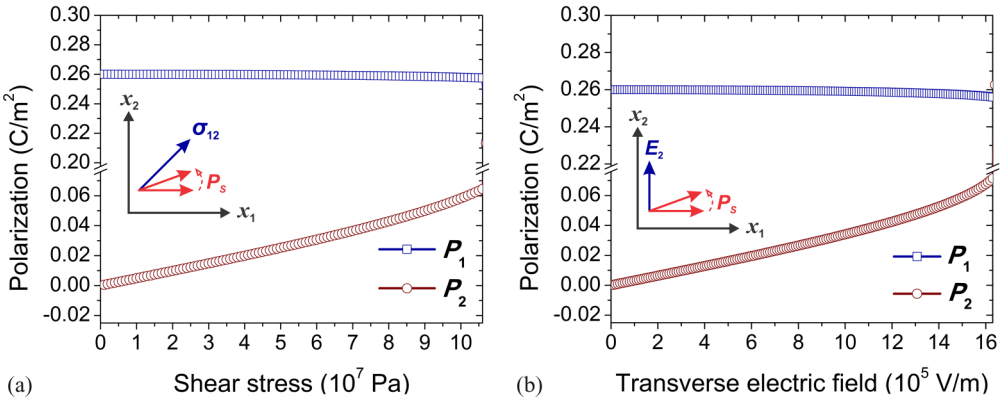

FIG. 5. (Color online) (a) The ferroelectric polarization in $BaTiO_3$ as a function of applied shear stress σ_{12}. (b) The ferroelectric polarization in $BaTiO_3$ as a function of applied transverse electric field E_2.

transient intermediate in the process and disappears at the end. However, during the transition the volume fraction of M_C phase can reach values as high as 90%, illustrating the polarization rotation mechanism of thermal inter-ferroelectric transitions.

Next, the equilibrium structure at 240 K is heated to 298 K. The relaxation process during heating [Fig. 4(b)] is generally the reverse of what occurs upon cooling. The M_C phase domains nucleate at the O domain walls, and grow along the ⟨110⟩ direction in the pseudocubic coordinate system. After 200 time steps, almost all the O domains have transformed to M_C domains. The majority of the M_C phase then suddenly transforms to the T phase after around 300 steps. The remaining M_C domains continue to shrink. After 10 000 steps, the system approaches equilibrium. The system as a whole recovers its original T domain structure, with only few small M_C domains persisting near the domain walls. The evolution of the volume fractions of the different phases during this temperature cycling process are shown in Fig. 4(b). Clearly, the M_C phases only exist as transient intermediates in this process, becoming almost extinct at equilibrium. An interesting feature of the M_C phase is that its domain walls are curved (i.e., follow irrational crystallographic planes), in contrast to the straight walls of the T phase and the O phase. Although the P_s of the M_C phase deviates from those of the T and O phases, the magnitude of this deviation at M_C/T or M_C/O domain walls is very small. The spontaneous strain tensors of the M_C phase and the parent phase (T or O) are almost identical. Therefore, the elastic anisotropy between the M_C and T or M_C and O phases is weak. As a consequence, the domain walls of M_C/T and M_C/O have no preferred orientations. This feature was also confirmed by experimental observations [25].

IV. MONOCLINIC PHASE STABILIZED BY COMPLEX DOMAIN STRUCTURES

As mentioned in the Sec. I, one important feature of the TPB is a flattened free energy profile. Thus, by applying an external shear stress or transverse electric field, the monoclinic phase can be easily stabilized. Although the emergence of monoclinic phases was discussed within the framework of eighth-order free energy by Vanderbilt and Cohen [24], the effects of applied strain, stress, and electric field were not considered. Here, we use $BaTiO_3$ single domain as an example and show that external stresses and/or electric fields can stabilize polarization rotation and thus, monoclinic phases.

We start from the Gibbs free energy of ferroelectrics, which can be obtained from the Helmholtz free energy (1) through a

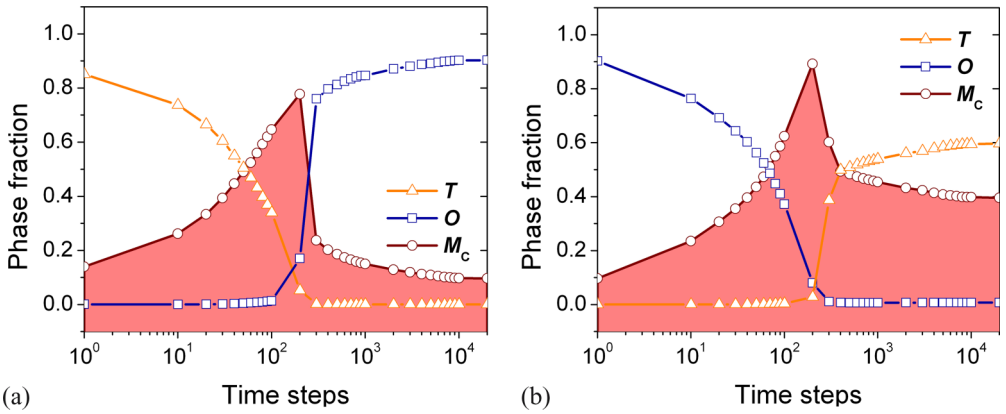

FIG. 6. (Color online) Volume fraction evolution of complex domain system with orthogonal twins in $BaTiO_3$ during temperature cycling. (a) Cooling from 380 to 240 K. (b) Heating from 240 to 298 K.

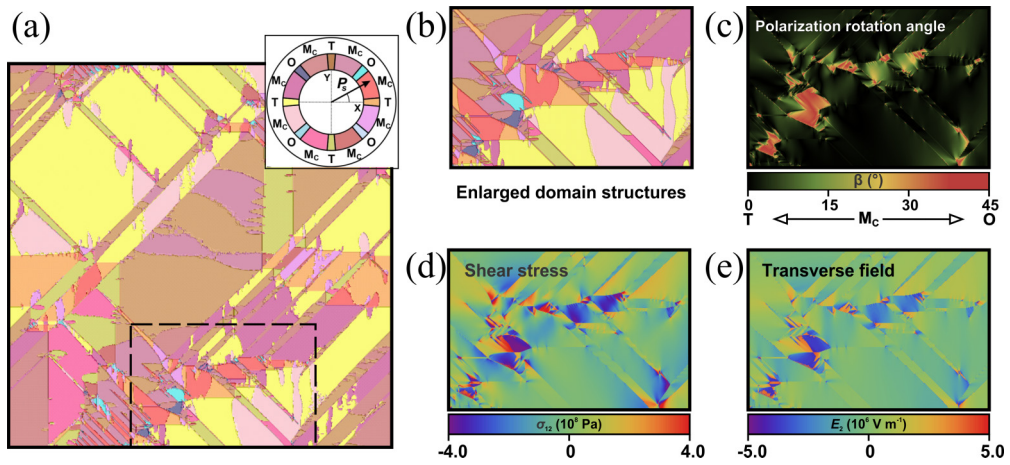

FIG. 7. (Color online) Domain structures in orthogonally twinned $BaTiO_3$ at 298 K after temperature cycling [25]. (a) Stable domain structure after equilibration at room temperature. (b) The zoomed-in domain structures shown in the dashed box of (a). (c) Polarization rotation angle. (d) In-plane shear stess σ_{12} of each domain. (e) Transverse electric field E_2, perpendicular to the polarization and in the plane of the image within each domain.

Legendre transform, i.e.,

$$G = F - \frac{\partial F}{\partial \varepsilon_j}\varepsilon_j = F - \sigma_j \varepsilon_j. \tag{4}$$

Assuming that the initial T structure has the polarization along x_1 direction ($P_1 \neq 0$ and $P_2, P_3 = 0$), the polarization change as the response to a shear stress σ_{12} or an electric field E_2 can be evaluated by minimizing the Gibbs free energy with respect to P_1 and P_2. The result is plotted in Fig. 5. The effects of both external factors are quite similar. The polarization rotation angle shows quasilinear dependence on the stress and electric field if the rotation angle is small ($<\sim 15°$). Upon further increase, the polarization discontinuously jumps to the direction corresponding to the O phase, with a critical point at $\sigma_{12} = 1.06 \times 10^8$ Pa, and $E_2 = 1.6 \times 10^6$ V/m, respectively [outside of the horizontal scales of Figs. 5(a) and 5(b), respectively]. These results demonstrate the possibility of stabilizing a monoclinic phase through incorporation of transverse stress and electric field in a typical ferroelectric system.

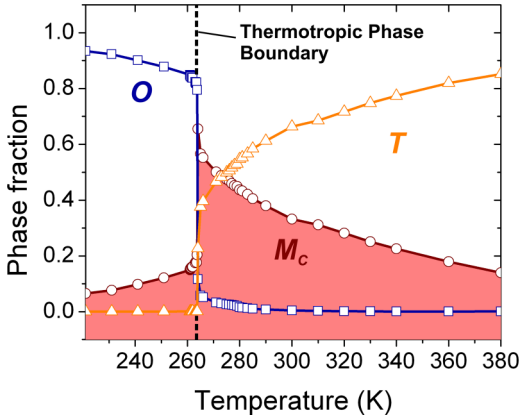

FIG. 8. (Color online) Thermotropic phase boundary of $BaTiO_3$ with orthogonal twinned domain structures (complex domain system).

In the following, we show that by introducing internal competing interactions (orthogonally twinned in-plane domains, or a complex domain configuration) to the $BaTiO_3$ domain structures, the kinetically intermediate M_C phase can be thermodynamically stabilized even far into the thermal O and T regimes. Under these circumstances, the conventional distinct inter-ferroelectric transition temperature is thus expanded to a TPB that spans a substantial thermal range.

In order to sustain a large multidomain structure in the periodic computational cell, we increase the system size to $1024\Delta x \times 1024\Delta x \times 4\Delta x$, with a grid spacing of $\Delta x = 1.8$ nm. To obtain an initial orthogonally twinned multidomain structure in $BaTiO_3$, we seed two small sets of perpendicular tetragonal twins within the simulation system, fill the rest of the grid with thermal noise, and then allow the system to evolve at 380 K until equilibrium is reached. We thus obtain

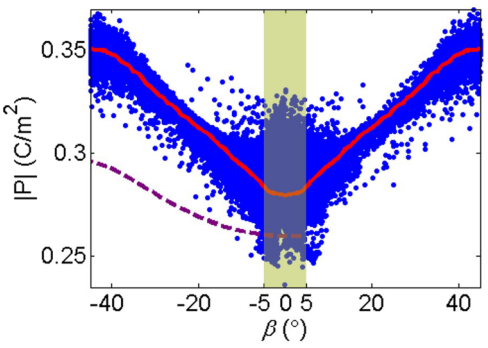

FIG. 9. (Color online) Magnitude of the polarization as a function of the polarization rotation angle, β, in the stabilized phase-field complex domain system at 298 K. The red line is the average polarization value as a function of β. The points within the shaded window (β ranging from $-5°$ to $5°$) are defined as tetragonal phase in this work. The dashed line is the magnitude of the polarization as a function of β on the polarization rotation path at 298 K, similar to Fig. 2(b).

the desired stable domain structures with orthogonal twinned domains. Next, we subject the obtained domain structures to a temperature cycle.

The temporal evolution of the orthogonally twinned domain structure shows some general similarities to that observed for the simple domain structure discussed above. As shown in Fig. 6, the volume fraction of the M_C phase initially increases with time, reaching a peak value in the middle of each transition process, and then decreases until the system reaches equilibrium. As in the previous case, the M_C phase occurs as a transient intermediate phase across the thermal phase transition. By contrast, however, in the case of the complex domain structure, the M_C phase persists in significant volume fractions. As shown in Fig. 6(a), initially the orthogonal tetragonal twins give rise to a stable M_C phase volume fraction of ~28%. Although this equilibrium M_C volume fraction drops to ~10% in the O regime (at 240 K), it increases to an equilibrium fraction of ~38% after reheating to room temperature [Fig. 6(b)]. The resulting room temperature domain structure is depicted in Fig. 7(a). As can be seen from both Figs. 7(a) and 7(b), the M_C phase mostly populates the regions where the sets of the orthogonal tetragonal twins meet. The corresponding shear stress σ_{12} and transverse field E_2 distribution of the same enlarged area is shown in Figs. 7(d) and 7(e), respectively. Comparison with the polarization rotation angle plot in Fig. 7(c) reveals a strong correlation between these three quantities, which strongly supports the notion of the shear stress and transverse field being responsible for stabilizing the monoclinic M_C phase. In the Appendix, we show that the monoclinic phase can also be stabilized by complex domain structures in $KNbO_3$. Thus the domain-structure-stabilized monoclinic phase can be regarded as a general phenomenon.

The phase diagram in Fig. 8 is constructed by quenching the stabilized 380 K domain structure in the temperature cycle mentioned above to a variety of lower temperatures in a set of parallel simulations. In each of these simulations, the system is evolved until equilibrium is reached. The resulting volume phase fractions as a function of the equilibrium temperature are plotted. As shown in Fig. 8, the M_C phase possesses a minimum of 6.5% of the overall volume fraction throughout 221 to 380 K. At 264 K and in thermodynamic equilibrium, the volume fraction of the M_C phase reaches a peak value of 65.5%. It then decreases with temperature but remains over 20% up to about 350 K. The thermotropic character of this ferroelectric phase boundary essentially originates from its domain structures. The orthogonal in-plane domain twins give rise to the in-plane shear stress (σ_{12}) and transverse electric field (E_2), which flatten the total free energy profile and stabilize the M_C phase.

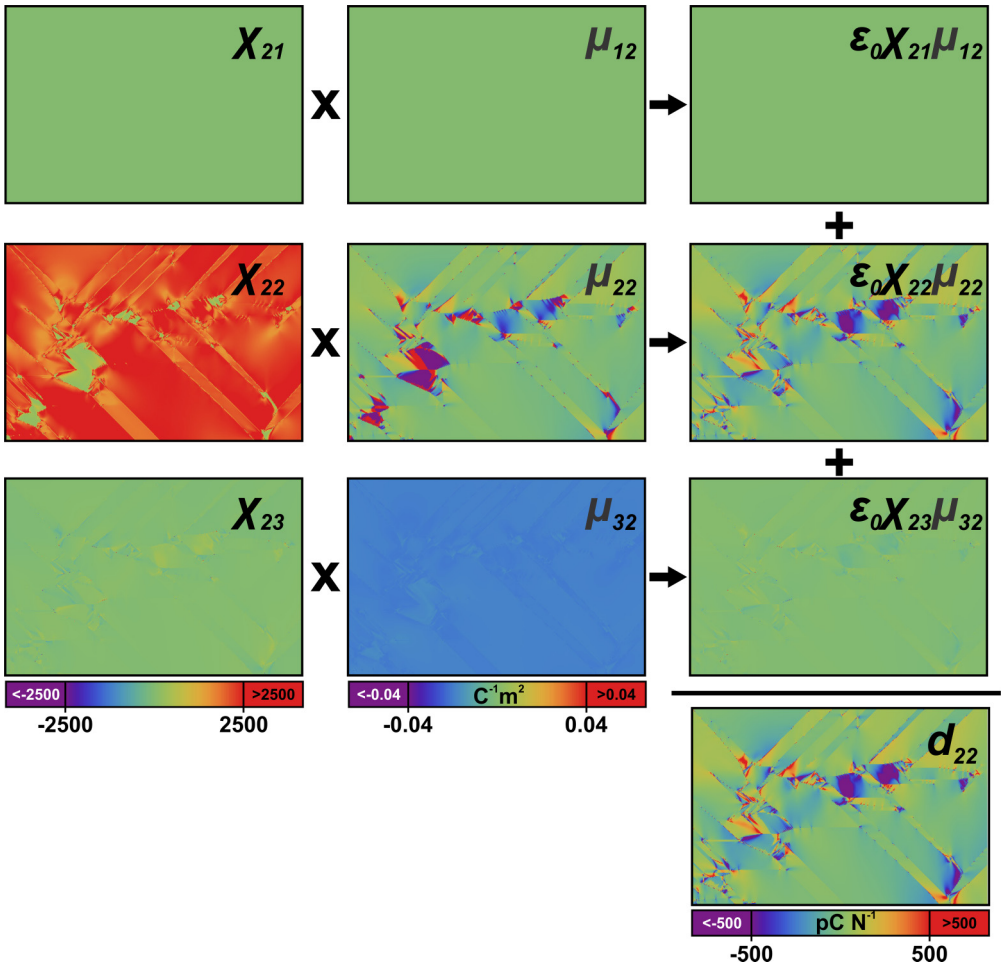

FIG. 10. (Color online) The calculation of d_{22} map from dielectric susceptibility χ and piezoelectric coupling coefficients μ.

V. DISCUSSION

In the previous two sections, we studied the role of domain structures on the stability of the monoclinic M_C phase during the thermal inter-ferroelectric T-O transitions. While the M_C phase appears only as a transient intermediate in the simple domain system, it can be stabilized over a wide temperature range and exists within a thermotropic phase boundary in the orthogonally twinned complex domain system. It should be noted that the thermodynamic analysis of the *external* field/stress stabilized monoclinic phase in Sec. IV is based on the *single domain* assumption. In contrast, in the complex domain system discussed in Sec. IV, the transverse electric field [Fig. 7(e)] and shear stress [Fig. 7(d)] are *internal*. They are inherently introduced by the domain structure. The polarization, electric field, and the stress are dependent on each other. Therefore, the stabilization of the monoclinic phase in a complex domain system is not a simple isolated incident but rather a complex emergent phenomenon. In order to study the features of the monoclinic phase stabilized by complex domain structures, we perform statistical analysis of the obtained domain structures from phase-field simulation shown in Fig. 8(b).

Figure 9 is the statistical plot of the magnitude of the polarization as a function of the polarization rotation angle, β, for all the grid points in the stabilized phase-field complex domain system at 298 K [Fig. 8(b)]. The complex system shows polarization properties that are distinct from those of the simple system. Specifically for the T phase (β ranging from $-5°$ to $5°$), 95% of the grid points in Fig. 7(b) have a polarization value within the range of 0.265 C/m^2 to 0.305 C/m^2, which is larger than the 0.26 C/m^2 observed in the simple domain system. The reason for this is twofold. On the one hand, the characteristic flattened free energy profile of TPBs facilitates the shifting of the local minimum by electric field and/or stress. On the other hand, the inherent competing interactions resulting from orthogonal in-plane domain twins introduce internal electric fields and stresses in the whole system, which further pushes the polarization away from its nominal equilibrium value. As the polarization angle, β, increases, the difference becomes more pronounced. This is consistent with the maps shown in Fig. 7: The area with higher polarization rotation angle is correlated with the area with larger transverse electric field and/or shear stress.

In addition to the increased polarization magnitude, the piezoelectric properties are also considerably modified in the complex system. The spatial distribution of the piezoelectric properties in the complex domain system is calculated the same way as in Ref. [25]. First, we extract the local electric field $E_i(\mathbf{r})$ and stress $\sigma_j(\mathbf{r})$ components from each spatial position $\mathbf{r}$. Then, with the extracted electric field and stress as external control parameters we perform independent single domain simulation to get the equilibrium polarization for each spatial position. In accordance with the standard crystal physics axes adopted for T phase [40], the local coordinate system is defined such that the largest absolute component of the polarization P_s is along the x_3 direction, and the x_1 axis is always along the [001] direction (out of the plane of the image). The local in-plane x_2 direction is orthogonal to x_3, complementing the orthogonal right-handed coordinate system. Then following the standard thermodynamic calculations [41], the piezoelectric coefficients of each spatial position $\mathbf{r}$ are calculated. As an example, Fig. 10 graphically demonstrates the calculation procedure of the piezoelectric coefficient d_{22}. Clearly, the dielectric coefficient χ_{22} and

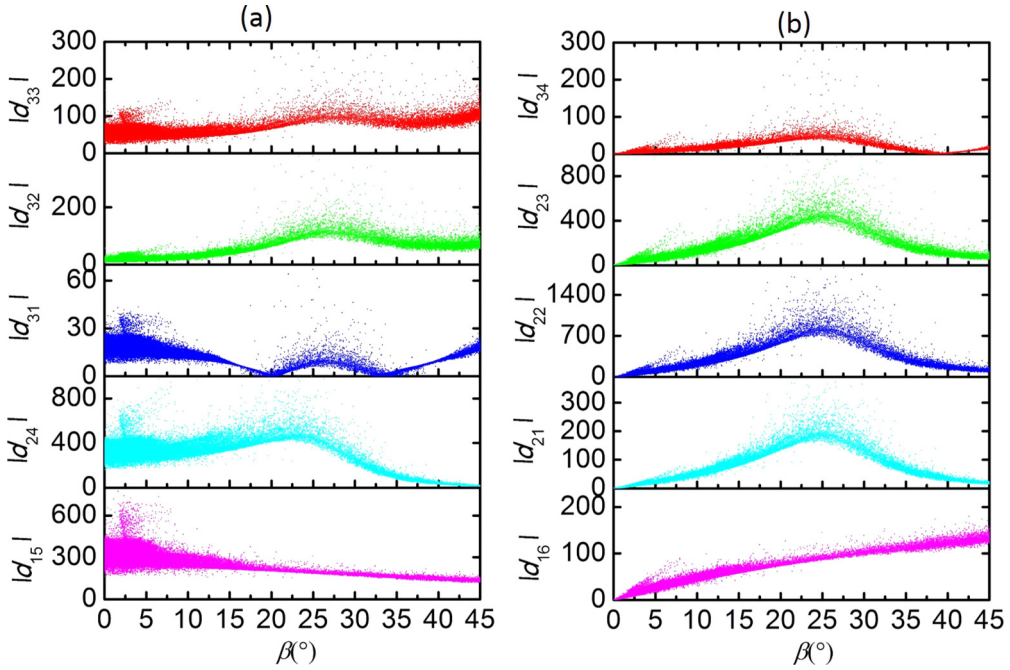

FIG. 11. (Color online) Piezoelectric coefficients d_{ij} as a function of the polarization rotation angle for the complex domain system shown in Fig. 7(b) at room temperature. (a) The nonzero components active in both the T and M_C phase. (b) The nonzero components active only in M_C phase and O phase.

the piezoelectric coupling coefficient μ_{22} are larger than the other components, respectively. Hence, d_{22} is dominated by the product $\chi_{22}\mu_{22}$. The emergence of d_{22} at TPB is, therefore, attributed to two reasons: The enhancement of dielectric permittivity χ_{22} is due to the flattening of the free energy, while the emergence of the coupling coefficient μ_{22} is probably due to the polarization rotation induced nonzero polarization component. The spatial maps of all calculated piezoelectric $|d_{ij}|$ coefficients in the complex domain system are presented in Ref. [25]. As demonstrated in Ref. [25], nonzero piezoelectric tensor components (d_{16}, d_{21}, d_{22}, d_{23}, and d_{34}) emerge in the M_C phase in addition to those that exist in both the T phase and M_C phase (d_{15}, d_{24}, d_{31}, d_{32}, and d_{33}). In order to analyze the piezoelectric properties in the complex domain system, we calculate all the d_{ij} coefficients and their corresponding polarization rotation angle in each grid point and plot them statistically in Fig. 11. Clearly, the piezoelectric properties of the M_C phase are very different from those of the T state. The monoclinic phase stabilized by the TPB processes exhibits strong and unique piezoelectric components that are missing in its neighboring T and O phases. In addition, almost all the piezoelectric coefficients except d_{15} and d_{31} are enhanced remarkably. In particular, $|d_{21}|$, $|d_{22}|$, and $|d_{23}|$, which are originally zero in the T phase, reach values as large as ~200, ~800, and ~450 pC/N respectively, when the polarization rotation angle is around 25° for the M_C phase. These elements may help to explain the enhanced piezoelectric properties of $BaTiO_3$ with engineered domain structures [16,17,42].

VI. SUMMARY

In this paper, we use the phase-field method to investigate monoclinic phases arising from thermal inter-ferroelectric phase transitions. Monoclinic phases are found to be kinetic intermediates in the T-O or O-R ferroelectric transitions. These transitional phases are found to be stabilized in equilibrium by introducing competing interactions in twinned multidomain structures. As a result, the conventional well-defined transition temperature is broadened into a thermotropic phase boundary region, which covers a substantial temperature range. The shear stress and transverse field inherently generated by the domain twinning are found to be key to the stabilization of these monoclinic phases. Concurrent with the observed symmetry reduction, the piezoelectric properties of the ferroelectric changes in the monoclinic phase are also found to be enhanced. New piezoelectric tensor components are allowed by the monoclinic symmetry, and piezoelectric properties become strongly dependent on the polarization direction, showing significant local enhancements. Our simulation results agree very well with recent experimental observations and may be used as a guide in designing novel ferroelectric phases and tuning piezoelectric properties.

ACKNOWLEDGMENTS

This work was supported by the U.S. National Science Foundation (NSF) through Grants No. DMR-0820404, No. DMR-1006541, and No. DMR-1210588. The computer simulations were carried out on the Lion-X and CyberSTAR clusters at the Pennsylvania State University, in part supported by instrumentation (CyberSTAR Linux cluster) funded by the NSF through Grant No. OCI-0821527.

APPENDIX: MONOCLINIC PHASE IN $KNbO_3$

The TPB of $BaTiO_3$ is near the T-to-O phase transition temperature. By analogy, we could anticipate the existence of an analogous monoclinic phase near the O-to-R phase transition temperature of $KNbO_3$ due to a similarly flattened energy profile. In this three-dimensional (3D) system, the simulation was performed at room temperature (298 K), using a 3D discretized mesh of size $256\Delta x \times 256\Delta x \times 256\Delta x$, with a grid spacing of $\Delta x = 1.0$ nm. Recently, Lummen *et al.* reported the experimental observation of monoclinic phases in $KNbO_3$ single crystals near 90° orthorhombic domain walls [25]. Here, we construct analogous initial domain structures, shown in Fig. 12(a), where [101] and [10$\bar{1}$] domains form 90° domain walls; while [0$\bar{1}\bar{1}$] domains form 60° and 120° domain walls with [10$\bar{1}$] and [101] domains, respectively. (We use the direction of polarization to denote each domain.) Marton *et al.* identified the mechanically compatible and electronically neutral domain walls in the isostructural orthorhombic phase of $BaTiO_3$ [43], which revealed that the 120° O domain wall is a crystallographic wall but the 60° O domain wall is not. As a result, the domain structure in Fig. 12(a) is accompanied by internal mechanical stress, which leads to the existence of monoclinic phase in the equilibrated domain structure, as shown in Fig. 12(b). In Fig. 12(b), the monoclinic phase (labeled in red) is defined by a polarization direction that deviates from any of the 12 orthorhombic polarization directions by more than 5°. The stress components σ_{22} and σ_{23} of the (010) plane [the front surface of Fig. 12(b)] are shown in Figs. 12(c) and 12(d). Both the stress components are very strong at the tip of [0$\bar{1}\bar{1}$] domains, which are crucial to stabilize the monoclinic phase. The existence of a stabilized monoclinic phase in twinned $KNbO_3$ suggests the generality of the thermotropic mechanism in inter-ferroelectric phase transitions.

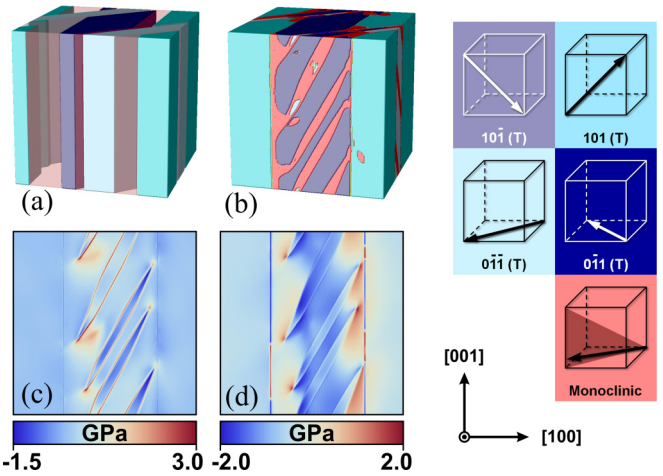

FIG. 12. (Color online) Phase-field simulation of $KNbO_3$. (a) Initial domain structures (the transparent red represents the noise); (b) final domain structures (the polarization direction of each domain is listed on the right); and (c), (d) the stress component σ_{22} (c) and σ_{23} (d) for the front surface of (b).

[1] F. Jona and G. Shirane, *Ferroelectric Crystals* (Dover, Mineola, NY, 1993).

[2] T. M. Shaw, S. Trolier-McKinstry, and P. C. McIntyre, Annu. Rev. Mater. Sci. **30**, 263 (2000).

[3] S. Trolier-McKinstry and P. Muralt, J. Electroceram. **12**, 7 (2004).

[4] R. Guo, L. E. Cross, S.-E. Park, B. Noheda, D. E. Cox, and G. Shirane, Phys. Rev. Lett. **84**, 5423 (2000).

[5] H. Fu and R. E. Cohen, Nature (London) **403**, 281 (2000).

[6] B. Noheda, D. E. Cox, and M. S. Centre, Phase Transitions **79**, 5 (2006).

[7] D. Viehland, J. Am. Chem. Soc. **89**, 775 (2006).

[8] B. Noheda, D. E. Cox, G. Shirane, R. Guo, B. Jones, and L. E. Cross, Phys. Rev. B **63**, 014103 (2000).

[9] B. Noheda, J. A. Gonzalo, L. E. Cross, R. Guo, S.-E. Park, D. E. Cox, and G. Shirane, Phys. Rev. B **61**, 8687 (2000).

[10] B. Noheda, Curr. Opin. Solid State Mater. Sci. **6**, 27 (2002).

[11] M. Ahart, M. Somayazulu, R. E. Cohen, P. Ganesh, P. Dera, H. Mao, R. J. Hemley, Y. Ren, P. Liermann, and Z. Wu, Nature (London) **451**, 545 (2008).

[12] K. J. Choi, M. Biegalski, Y. L. Li, A. Sharan, J. Schubert, R. Uecker, P. Reiche, Y. B. Chen, X. Q. Pan, V. Gopalan, L. Q. Chen, D. G. Schlom, and C. B. Eom, Science **306**, 1005 (2004).

[13] O. Diéguez, K. M. Rabe, and D. Vanderbilt, Phys. Rev. B **72**, 144101 (2005).

[14] D. Lee, R. K. Behera, P. Wu, H. Xu, Y. L. Li, S. B. Sinnott, S. R. Phillpot, L. Q. Chen, and V. Gopalan, Phys. Rev. B **80**, 060102(R) (2009).

[15] J. Sinsheimer, S. J. Callori, B. Bein, Y. Benkara, J. Daley, J. Coraor, D. Su, P. W. Stephens, and M. Dawber, Phys. Rev. Lett. **109**, 167601 (2012).

[16] S. Wada, S. Suzuki, T. Noma, T. Suzuki, M. Osada, M. Kakihana, S.-E. Park, L. E. Cross, and T. R. Shrout, Jpn. J. Appl. Phys. **38**, 5505 (1999).

[17] S. Wada, K. Yako, H. Kakemoto, T. Tsurumi, and T. Kiguchi, J. Appl. Phys. **98**, 014109 (2005).

[18] S.-E. Park, S. Wada, L. E. Cross, and T. R. Shrout, J. Appl. Phys. **86**, 2746 (1999).

[19] D. Damjanovic, Appl. Phys. Lett. **97**, 062906 (2010).

[20] D. Damjanovic, J. Am. Ceram. Soc. **88**, 2663 (2005).

[21] D. Damjanovic, M. Budimir, M. Davis, and N. Setter, J. Mater. Sci. **41**, 65 (2006).

[22] M. Budimir, D. Damjanovic, and N. Setter, J. Appl. Phys. **94**, 6753 (2003).

[23] L. Liang, Y. L. Li, S. Y. Hu, L.-Q. Chen, and G.-H. Lu, J. Appl. Phys. **108**, 094111 (2010).

[24] D. Vanderbilt and M. H. Cohen, Phys. Rev. B **63**, 094108 (2001).

[25] T. T. A. Lummen, Y. Gu, J. Wang, S. Lei, F. Xue, A. Kumar, A. T. Barnes, E. Barnes, S. Denev, A. Belianinov, M. Holt, A. N. Morozovska, S. V. Kalinin, L.-Q. Chen, and V. Gopalan, Nat. Commun. **5**, 3172 (2014).

[26] Y. Yoshimura, A. Kojima, N. Tokunaga, K. Tozaki, and T. Koganezawa, Phys. Lett. A **353**, 250 (2006).

[27] H. Cao, C. P. Devreugd, W. Ge, J. Li, D. Viehland, H. Luo, and X. Zhao, Appl. Phys. Lett. **94**, 032901 (2009).

[28] C. Eisenschmidt, H. T. Langhammer, R. Steinhausen, and G. Schmidt, Ferroelectrics **432**, 103 (2012).

[29] L.-Q. Chen, Annu. Rev. Mater. Res. **32**, 113 (2002).

[30] L.-Q. Chen, J. Am. Ceram. Soc. **91**, 1835 (2008).

[31] Y. L. Li, L. E. Cross, and L. Q. Chen, J. Appl. Phys. **98**, 064101 (2005).

[32] L. Liang, Y. L. Li, L. Chen, S. Y. Hu, and G. Lu, Appl. Phys. Lett. **94**, 072904 (2009).

[33] A. G. Khachaturyan, *Theory of Structural Transformations in Solids* (Dover, Mineola, NY, 2008), p. 576.

[34] Y. L. Li, S. Y. Hu, Z. K. Liu, and L. Q. Chen, Appl. Phys. Lett. **81**, 427 (2002).

[35] A. K. Tagantsev, Ferroelectrics **375**, 19 (2008).

[36] Y. Zheng and C. H. Woo, Appl. Phys. A **97**, 617 (2009).

[37] L.-Q. Chen and J. Shen, Comput. Phys. Commun. **108**, 147 (1998).

[38] E. Fatuzzo, Phys. Rev. **127**, 1999 (1962).

[39] X. Q. Ke, D. Wang, X. Ren, and Y. Wang, Phys. Rev. B **88**, 214105 (2013).

[40] R. E. Newnham, *Properties of Materials: Anisotropy, Symmetry, Structure* (Oxford University Press, New York, 2004).

[41] M. J. Haun, E. Furman, S. J. Jang, and L. E. Cross, Ferroelectrics **99**, 13 (1989).

[42] S. Wada, K. Yako, K. Yokoo, H. Kakemoto, and T. Tsurumi, Ferroelectrics **334**, 17 (2006).

[43] P. Marton, I. Rychetsky, and J. Hlinka, Phys. Rev. B **81**, 144125 (2010).